ELSEVIER

Electroencephalography and clinical Neurophysiology 102 (1997) 307–315

Cardiac field effects on the EEG

G. Dirlich*, L. Vogl, M. Plaschke, F. Strian

Max Planck Institute of Psychiatry, Clinical Institute, Kraepelinstrasse 10, 80804 Munich, Germany

Accepted for publication: 21 October 1996

Abstract

The electrical field of the heart propagates throughout the entire body and causes changes in the surface potentials on the scalp that are superimposed on brain electric signals. When heart cycle-related EEG averaging is performed, e.g. in order to measure heart cycle-related brain potentials, the effects of the cardiac electrical field result in a high-amplitude artifact in the surface potentials. The topographic and temporal distributions of the cardiac field artifact were measured in 9 normal subjects. In addition, the effects of head-turning on the field were investigated. The electrocardiac artifact is most prominent during the QRS complex and during the T wave of the heart cycle. In both cases it is distinctly asymmetrical in relation to the hemispheres. A comparison of the scalp potentials and a computed vector ECG showed the 3-dimensional nature of the artifact. Non-computational strategies for the handling of the ECG artifact are discussed. A proper separation of the effects of the cardiac electrical field from heart cycle-related brain potentials is a prerequisite for the study of heart cycle-coordinated brain potentials. © 1997 Elsevier Science Ireland Ltd.

Keywords: Cardiac electrical field; Vector electrocardiogram; Electrocardiographic body surface mapping; Cardiosynchronous brain activity; Heart evoked potentials

1. Introduction

Heart cycle-related EEG averaging has been used in studies on interoceptive processes. The approach was first reported by Schandry et al. (1986) and by Jones et al. (1986). Analogously to sensory evoked potentials brain potentials caused by internal stimuli recurring with the heart cycle were searched. The R peak in the ECG was used as temporal reference for the EEG averaging.

However, the results of heart cycle-related EEG averaging are strongly affected by an artifact caused by the cardiac electrical field. This field propagates throughout the body and can be measured at any location on the body surface, including the scalp. The cardiac field artifact (hereafter referred to as CFA) in the EEG is not relevant in most clinical and experimental situations because of its small amplitude. However, in connection with heart cycle-related EEG averaging it turns out to be a central problem. This has been recognized already in the first reports and is a major methodological issue in recent studies (Jones et al., 1988; Riordan et al., 1990; Schandry and Weitkunat, 1990; Montoya et al., 1993).

In some of these studies computational methods were used to remove the CFA from the averaged EEG data. Information about the cardiac electrical field was measured at one location, the tip of the nose, and used to estimate the artifact amplitude at other locations (Schandry and Weitkunat, 1990; Montoya et al., 1993). Statistical methods have also been used to remove the CFA (Schandry et al., 1986). In other reports no information is given on how the CFA was treated (Jones et al., 1988; Riordan et al., 1990).

Heart cycle-related EEG averaging has also been used within another paradigm by Walker and Sandman (1982) and Sandman et al. (1992) in the search of variations of evoked potentials with the phase of the cardiovascular cycle. They described the impact of the cardiac electrical field on the averaged EEG as a factor of only minor importance.

The arguments in the literature concerning the handling of the CFA and its effects on heart cycle-related averaged EEG are inconsistent and contain major disagreements

* Corresponding author. Tel.: +49 89 30622226; fax: +49 89 30622 200; e-mail: dirlich@mpipsykl.mpg.de.

PII S0921-884X(96)96506-6

about the magnitude and the spatio-temporal pattern of the artifact.

Observational data depicting the complete spatio-temporal pattern of the artifact and allowing empirical validations of the suggested methods for handling the artifact are lacking so far. Still, it is an open question, whether the available methods can eliminate or at least reduce the CFA sufficiently so that a proper separation of the effects of the cardiac electrical field and brain potentials can be achieved.

There are numerous reports on the potential distribution generated by the cardiac field on the body surface. However, the reports on body surface mapping of the cardiac field are mostly related to cardiological questions. This explains why the measurements are restricted to the torso (He and Cohen, 1992; Lorange and Guirajani, 1993; Medvegy et al., 1993; Turzova et al., 1994). The reports contain no quantitative data about the cardiac field potentials on the scalp. Therefore, data on the topographic distribution of the effects, of the electrocardiac field on the scalp and on its temporal dynamics are not available from the cardiological literature. The goal of the present study was to collect such data. In addition, non-computational approaches of handling the CFA were explored.

In the present context, scalp potentials can be conceived of as containing two components: (1) heart-related brain potentials, and (2) the CFA. In our study we attempted an experimental separation of the two components by varying the spatial relations between the sources of the two components, the heart and the brain, by means of head turns. We expected basically unaltered brain potentials but possibly modified CFA patterns.

The expectations concerning the effects of head turns were influenced by the following considerations: If local electrical properties of the body tissue are the sole factor determining the field propagation, then the field propagation would appear to be attached to the tissue, and a turn of the head should twist the field; the CFA should remain essentially unchanged. If, in contrast, the head is moved through the field a head turn should change the location of the head relative to the field; rotation-like changes in the artifact should result.

The propagation of the field is a problem of volume conduction through body tissue, governed by the laws of electrodynamics (Scherg, 1990; Hämäläinen et al., 1993). However, the field geometric properties of body tissue are complex and not known in detail. Computational derivations of the potential distribution of the CFA on the scalp from ECG information appear to be impossible at present and empirical approaches are necessary to understand the influence of the CFA on heart cycle-related averaged EEG.

2. Methods

Nine healthy young men aged 20–29 years took part in the study. A careful medical evaluation revealed no heart disease, regular auscultation states, no brady- or tachycardias and normal ECGs with respect to durations, waveforms and intervals. Prior to the experiment the subjects were informed about the purpose of the study and the experimental protocol.

The experiments took place in an electrical- and sound-shielded laboratory. The subjects were seated in a chair with a nearly vertical back support. The chair stood on a turntable. Behind the turntable was a head support. The head support and the chair could be adjusted so that the subjects could assume a relaxed position with their head against the head support and their upper body in an upright position. In this position, the vertical extension of the axis of rotation of the platform fell together with the axis of rotation of the head. The subjects were instructed to watch a silent movie on a television set 2 m in front of them. While the subjects kept their head in a fixed position in relation to the room and to the television set, their body could be rotated by turning the platform with the chair to the left or to the right without causing the subjects any discomfort. Three head orientation conditions were introduced: 'straight', where the sagittal axes of the head and the trunk were identical, 'left', where the head was 45° to the left of the trunk, and 'right', where the head was 45° to the right. In pilot experiments turns of 45° were found to be achievable without any discomfort in all subjects.

The experiment was carried out as a sequence of 9 blocks of 400 s duration, each with continuous data recording and short breaks between the blocks. In each block there was a new head orientation condition. For each subject a different pseudo-random sequence of the three conditions was used. Over the group each condition occurred with the same frequency (33%) at any position in the block sequence.

The instruction to watch the silent movie was given to distract the subjects' attention from their heart action so as to reduce the likelihood of perception-related evoked potentials (Montoya et al., 1993). In addition, the subjects were asked to avoid eye movements and eyeblinks as much as possible and to remain alert.

Three types of data were recorded: (1) two standard ECG limb leads, from the right arm and from the left leg; (2) four ECG chest leads, with electrodes positioned as follows: one in the fifth intercostal space (ICS) at the midaxillary line on the right side of the chest and one on the left, one at the level of the fifth ICS horizontally on the midsternal line and one at the same level on the midspinal line (Slant and Alexander, 1994); (3) 26 EEG channels according to the augmented 10-20 system (Jasper, 1958). Cz was the common reference for all three types of channels. Data were collected by a DC 32-channel recording system (Schwind Medizintechnik, Erlangen, Germany) at a sampling rate of 500 Hz and low-pass filtered at 100 Hz; the amplitude resolution was 0.3 μV (Heuser-Link et al., 1992).

The difference between the two limb leads yields an

ECG signal that was used to mark the R peaks by a peak- and maximum slope-detecting algorithm as reference events for the averaging procedure; the difference between the two midaxillary leads is an estimate of the lateral cardiac field component; and the difference between the midsternal and midspinal leads is an estimate of the sagittal field component. The average of the 4 chest channels yields an estimate of the axial field component. With these data a vector ECG could be computed that conveys information about the three-dimensional shape of the cardiac field (Slant and Alexander, 1994).

The recorded data were visually screened for artifacts, namely movement, muscular and DC-drift artifacts. Time intervals with artifacts were excluded from the analysis. Eyeblink artifacts were detected and corrected computationally (Gratton et al., 1983). For the averaging procedure sweeps were defined starting 300 ms before the R peak, i.e. about 50 ms before the onset of the P wave, and ending 1200 ms after the R peak, so that at a frequency of 60 beats/min the postevent interval contained just one RR cycle.

For the R peak-related averaged data, correlations between the cardiac field components were computed. Multivariate regression analyses with estimations of the residual variance were performed to assess the predictive power of the cardiac field components for the scalp potentials. Spheric spline interpolation was used to obtain whole head views of the three-dimensional potential distribution at the head (FOCUS, MEGIS Munich, 1995). Scalp potential maps combined with information about the cardiac field components were used to illustrate the temporal dynamics of the CFA.

3. Results

The grand average of R peak-related averaged EEG from 9 subjects (a total of 12120 heart cycles, condition 'straight') is used here to describe the effects of the cardiac electrical field on the scalp potentials. Correlation coefficients between the three geometrically orthogonal components of the cardiac field, i.e. lateral, vertical and sagittal, are shown in Table 1. The values obtained in three time windows positioned in the QRS complex of the cardiac cycle demonstrate great variability. The presence of very high values indicates that the time courses of the cardiac field components are nearly free of random variability (see below and Fig. 3).

Two regression models were used: one-dimensional linear regression with one of the cardiac field components as the independent variable and three-dimensional linear regression with all three cardiac field components as independent variables. For each scalp channel the one-dimensional analyses yield the residual variances with each of the field components. These data allow an estimation of the predictive power of the field components at each scalp electrode position. A summary of these results is given in Table 1. The mean over all 26 scalp channels of the residual variance obtained in three time windows positioned in different phases of the cardiac cycle, namely in the RS interval, in the slope of the T wave and in the interval after the end of the T wave until the next P wave are shown. Of course, the marked differences between different electrode positions are not reflected by these data. However, the data demonstrate, that the lateral component of the cardiac field is the most effective one. The inclusion of the three field components in the regression analysis yields prominent reductions in the residual variances. In the first window, positioned in the RS interval, more than 99% of the mean residual variance can be explained by cardiac field influences. In the second window, positioned before the peak of the T wave, more than 80% of the variance still results from the cardiac field. However, in the last window, positioned in the interval between the T wave and the next P wave, only about 40% of the variance can be explained by the cardiac electrical field.

The time courses of the three field components and of four selected scalp potentials in Fig. 1 show (a) differences in amplitude and phase between the three field components, (b) great similarity in the shape of the time courses in the scalp channels to the field components during the PQRST segment of the cardiac cycle, and (c) a magnitude of the cardiac field artifact in the scalp channels exceeding all other variability in the scalp potential courses. Fig. 2 illustrates the three-dimensional effects of the cardiac electrical field at the peak of the T wave (244 ms) in the form of a whole head equipotential maps computed by the FOCUS-program using spheric spline interpolation.

A synopsis of R peak-related averaged standard ECG, vector ECG and scalp potentials demonstrates the topographic and temporal structure of the CFA and its correlation with the cycle of the cardiac field. In what follows data from one selected subject are used. The CFA is so promi-

Table 1

Summary of correlation and regression analysis

Window	Lateral–vertical	Lateral–sagittal	Vertical–sagittal	
Correlation coefficients				
−50–0 ms	0.96	−0.36	−0.10	
0–50 ms	0.97	−0.08	0.15	
50–100 ms	0.99	0.94	0.98	
	Lateral	Vertical	Sagittal	3-D
Mean residual variances				
0–50 ms	21.5	26.0	79.6	0.4
150–200 ms	28.3	28.3	28.6	17.6
450–500 ms	53.6	53.3	53.4	39.8

Correlation coefficients between the three components lateral, vertical and sagittal of the cardiac electrical field in three time windows ($t = 0$ at the R peak; grand average of 9 subjects). Mean values over 26 scalp channels of the residual variance in regression analyses (see text).

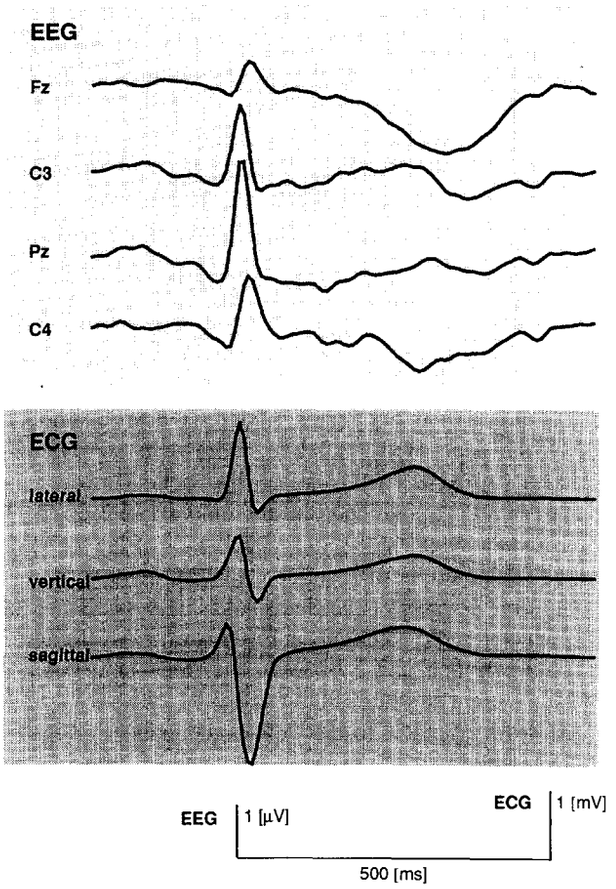

Fig. 1. R peak-averaged potential courses for the lateral, vertical and sagittal component of the cardiac field measured by four chest leads and Cz (lower part). R peak-related average-referenced scalp potentials at Fz, C3, Pz and C4 (upper part). Grand average of 9 subjects each of them contributing about 1200 sweeps. Head orientation 'straight'.

nent that a single case demonstration is appropriate. For subject 6, condition 'straight', data were recorded for 1209 s, 20 s of which were disturbed by artifacts and excluded from the analysis – 1382 RR cycles were analyzed. The average heart rate was 70 beats/min. The averaged standard limb lead ECG is shown in Fig. 3a. The temporal dynamics of the cardiac field is represented by averaged computed vector cardiograms shown from the lateral, frontal and bird's-eye perspective (Fig. 3b–d). The big loop represents the QRS complex at the beginning of the systole. The small loop represents the T wave in the diastole. (The shape of the vector diagrams of the other 8 subjects (not shown) differ markedly from each other during the QRS loop, whereas their variability during the T loop is quantitative rather than qualitative. All vector diagrams indicate normal individually varying orientations of the electric heart axis and normal heart function. The QRS loop in Fig. 3 comes close to the T loop twice in 3-dimensional space. But at the peak times of the R and T waves the respective heart vectors are far apart from each other in 3-dimensional space. This signifies marked dissimilarities in the cardiac field during the QRS complex and during the T wave at almost all times. (This was found to be true for all 9 subjects.) The orientation of the heart vector at the T peak can be roughly inferred from the graphs: the vector points to the front (Fig. 3b,d), to the left (Fig. 3c,d) and downward (Fig. 3b,c). (Similar orientations were found in all subjects.)

Particularly during the QRS complex and during a time interval around the peak of the T wave scalp potential maps show distinct high amplitude patterns. A few examples at selected time points demonstrate the typical patterns and their dynamics (Fig. 4). Here, Cz referenced scalp potential data were used. With Cz as reference the geometry of the map has a clear structure. The common feature of the maps is a partitioning of the 26 electrode locations into two clusters with no apparent relation to brain anatomy (e.g. the hemispheres). Several locations with small potentials separating the two clusters indicate the presence of a low potential region on which Cz, the common reference, lies. This region marks the intersection of an equipotential surface of the cardiac field in 3-dimen-

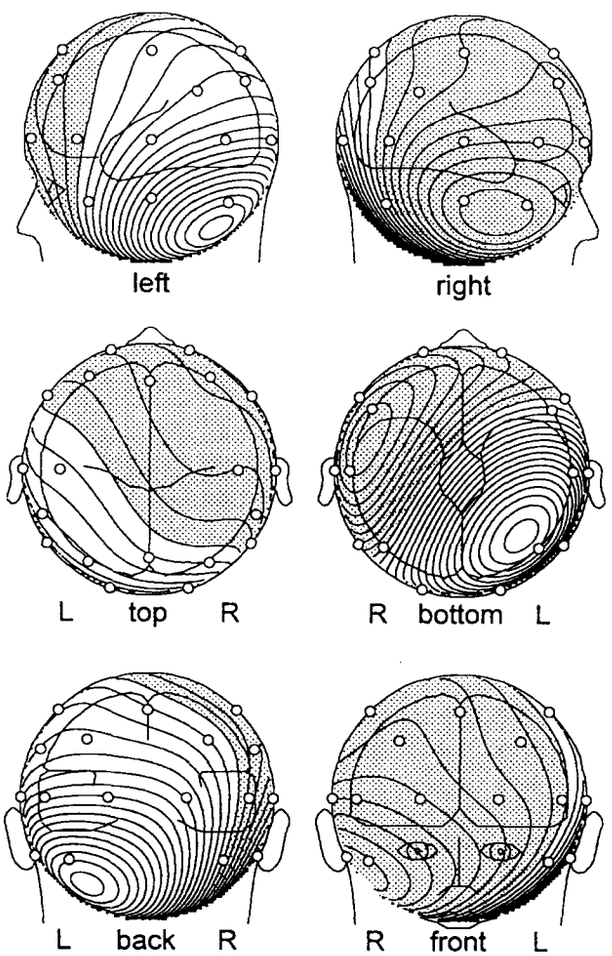

Fig. 2. Amplitude maps with different whole head views at the peak of the T wave (244 ms post R peak). Grand average (n = 9).

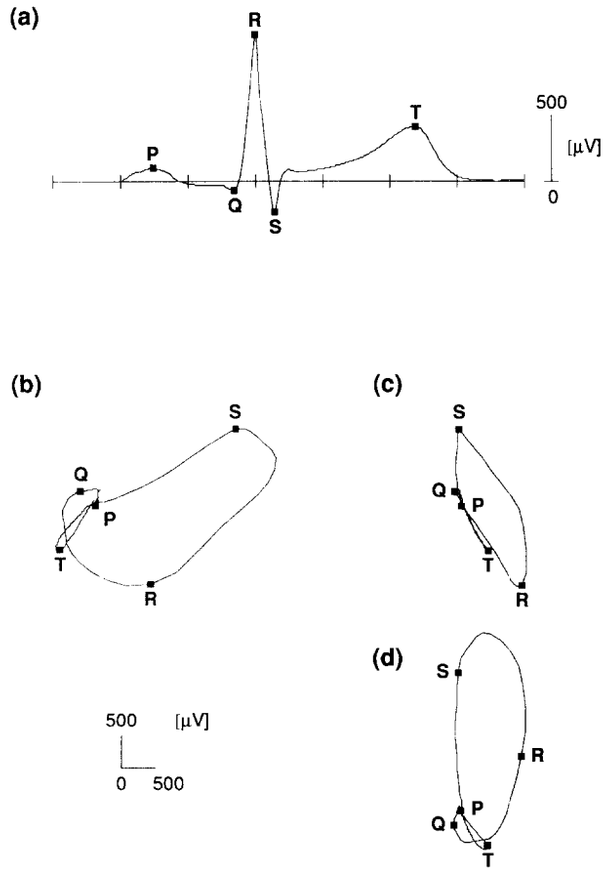

Fig. 3. R peak-averaged electrocardiographic data for subject 6 (condition 'straight'). (a) R peak-related averaged ECG: bipolar standard limb lead 'right arm–left leg'; (b) R peak-related averaged computed vector ECG: perspective from the left side of the body (profile, subject looking to the left) showing the axial–sagittal projection of the vector loop; (c) frontal perspective (subject looking towards the observer) showing the lateral-axial projection; (d) bird's-eye perspective (subject looking towards the bottom of the page), lateral-sagittal projection. The cardiac events P, Q, R, S and T are indicated by squares.

sional space with the surface of the head. One cluster of electrode location lies inside, the other outside this surface. Consecutive maps show rotation-like changes. At the time of the R peak (Fig. 4, top) rapid changes occur in both the ECG and in the scalp potentials: during a time interval of 24 ms the magnitude and orientation of the heart vector change markedly. The shift can be described as a counterclockwise rotation; 12 ms after the R peak its vertical component nearly disappears transiently. In the 3 potential maps a counterclockwise rotation of the pattern associated with the rotation of the heart vector is also apparent.

For the T wave (Fig. 4, bottom), the changes in the heart vector during an interval of 48 ms around the T peak are smaller; no marked changes occur in the potential maps. The maps around the T peak are also distinctly asymmetrical with respect to the hemispheres. In contrast to the relationship between the direction of the heart vector and the orientation of the potential map at the R peak, here the vector is always approximately parallel to the diagonal orientation of the potential pattern at the T peak. Although the size of the heart vector shrinks significantly from the first (-24 ms) to the last (24 ms) potential map, the potential pattern remains essentially the same. It is noteworthy that the vertical component of the cardiac field also remains nearly constant during this time interval.

The basic finding from the head turning experiment is distinct and can also be demonstrated by single case data. Several potential maps from subject 6 illustrate the influence of head turns (Fig. 5).

The cardiac field in the three conditions was very stable as indicated by the computed vector ECG: the magnitude of the heart vector (radius of the variable circle), its orientation in the horizontal plane (clock position) and the magnitude of its vertical component (vector at the left) are similar in the three conditions for both the R peak and the T peak. However, the potential maps at the R peak (upper row) are distinctly different in the three conditions: from 'left' to 'straight' to 'right' the patterns rotate on the scalp in the direction opposite to that of the head turn. A similar rotation can be seen in the maps at the peak of the wave (lower row).

A comparison of the data from the three head orientation conditions, showed marked effects in all 9 subjects. They were similar and hence group statistics are given hereafter. Ten of the 26 electrode positions, Fp1, F7, T3, T5, O1, O2, T6, T4, F8 and Fp2, form a ring. They are distributed at angles of 36° between adjacent positions around the head, lying in an approximately horizontal plane with similar vertical distances from Cz. A topographic representation of the group means ($n = 9$) at the 10 electrodes in condition 'straight' shows the diagonal partitioning (from T3, F7 to T4, T6) of the ring into a half circle with positive potentials and a half circle with negative potentials (Fig. 6a, upper part).

This pattern appears to be rotated somewhat in the other conditions, 'left' and 'right' (Fig. 6a, lower part). Estimates of the observed rotation angles (means of zero crossings of individual linearly interpolated potential courses along the ring) yield about 20° for the 'straight-left', and about 20° for the 'right-straight' comparison. This is 45% of the physical rotation angles in the conditions 'left' and 'right'. The rotations between the conditions are statistically significant for the comparison 'straight-left' (Wilcoxon signed ranks tests for the crossings from positive to negative and for the diagonally situated crossings from negative to positive potential values, $n = 9$, both $P < 0.01$) and for the comparison 'right-straight' (both $P < 0.01$).

In an analogous analysis at a latency of 244 ms, the mean group latency of the T peak yielded relations similar to those for the R peak (Fig. 6b). The rotation effects were significant for the comparison 'left-right' (both $P < 0.01$). Several differences in comparison to the R peak exist. (1) The means of the potentials have a smaller magnitude

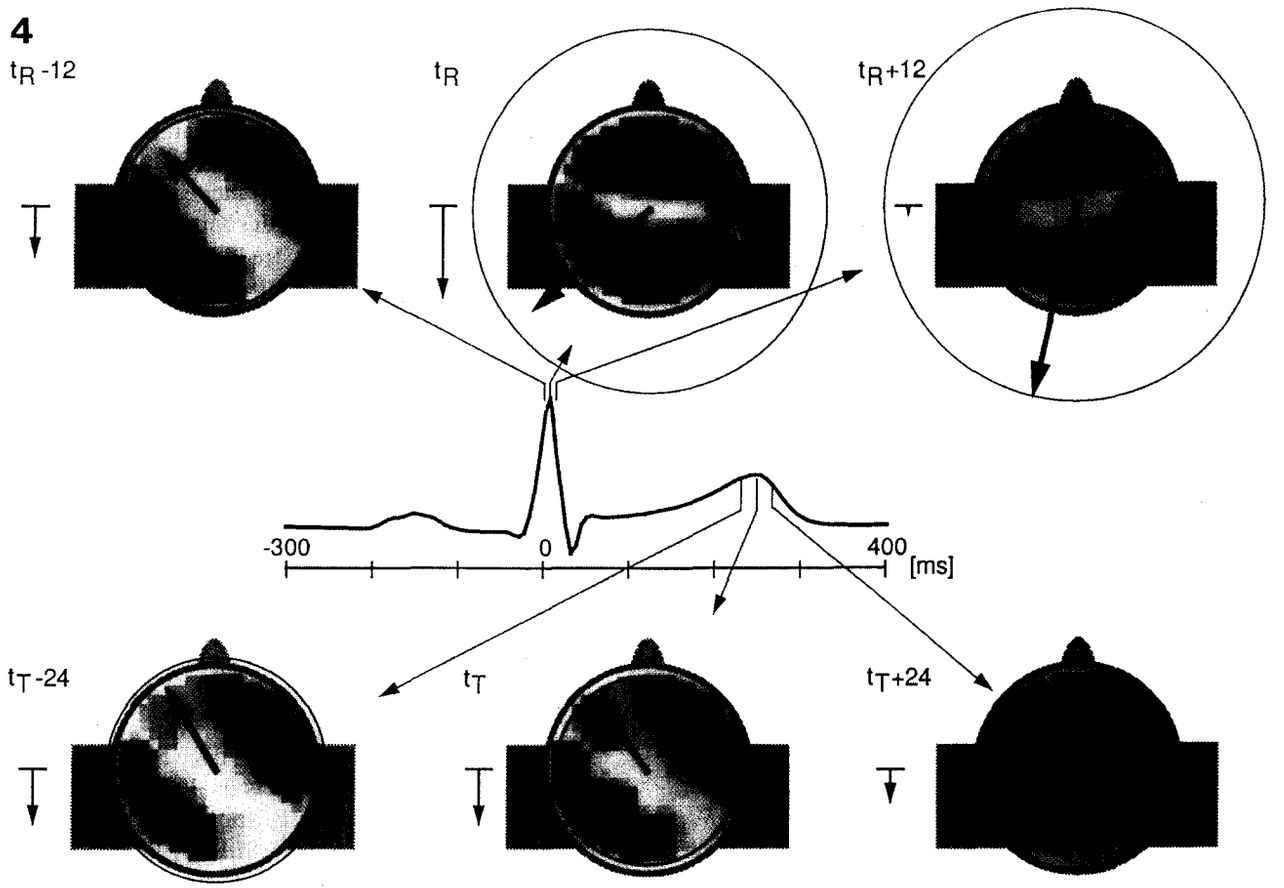

Fig. 4. R peak-related averaged electrocardiographic and EEG data for subject 6 in condition 'straight' at 3 time points around the R peak (t_R) (top) and at 3 time points around the T peak (t_T) (bottom). Selected time points in the QRS complex: t_R-12, t_R, t_R + 12 (ms), in the T wave t_T-24, t_T, t_T + 24 ms). The body-head schema indicates the head orientation 'straight' (in this representation the subject is looking towards the top of the page, in contrast to the perspective in d, which is usually used in vector ECG representations). Three electrocardiographic variables are represented: (1) a circle represents the instantaneous magnitude of the cardiac field dipole (scaling information in Fig. 5), (2) an arrow and its clock position indicates the instantaneous magnitude and orientation of the horizontal projection of the cardiac dipole, (3) the vertical arrow at the left of each schema shows the axial field component. Interpolated scalp potential maps based on averaged potentials in the 26 EEG channels with Cz as common reference. Scaling information in Fig. 5, red: positive, blue: negative.

(40%). (2) The orientation of the patterns is different: in the T wave it is rotated about 35° clockwise as compared to the R peak. (3) The entire potential course along the ring appears to be more negatively shifted for the T wave than at the R peak.

The interval beginning after the decay of the T wave and ending before the beginning of the next cardiac cycle is free of effects from the cardiac electrical field. The amplitude ratios between the cardiac potentials measured at the limb and chest leads and the CFA potentials at the scalp electrodes at the peaks of the R and T waves are about 100:1 in the electrode positions most affected by the CFA (Cb1 and Cb2), i.e. amplitudes of 1 mV at the ECG channels cause CFA amplitudes never exceeding 10 μV in any electrode position and subject. Thus, when the cardiac field has decayed to less than 30 μV during the post-T wave interval, CFA amplitudes of less than 0.3 μV can be expected. Based on this criterion for the 9 subjects, the practically artifact-free segments of the post T interval were measured. Its beginning ranged from 307 to 389 ms (mean: 349 ms) and its end ranged from 516 to 745 ms (mean: 628 ms). Hence for a mean duration of about 280 ms there is a CFA-free window in the post T interval.

4. Discussion

Cardiac cycle-related EEG averaging is a method for measuring heart cycle-related signals in the EEG. However, its application is hampered by an artifact originating from the cardiac electrical field. During certain phases of the heart cycle the magnitude of this artifact is distinctly greater than the expected magnitude of the searched brain potentials. The main result of the present study is a depiction of the spatio-temporal potential patterns on the scalp in relation to the cardiac field. The magnitude, shape and dynamic properties of the potential patterns indicate their

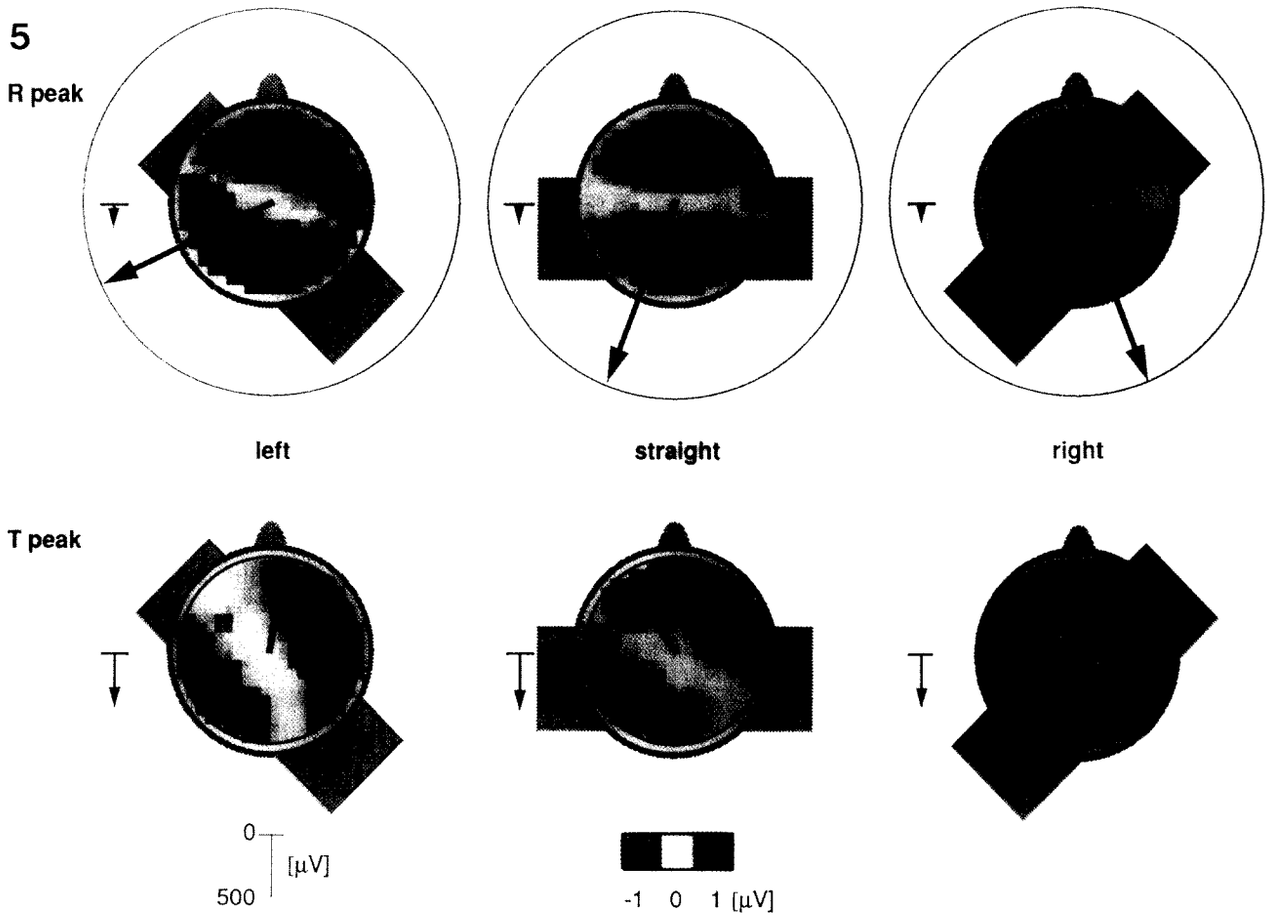

Fig. 5. R peak-related averaged electrocardiographic and scalp potential maps for subject 6 in the head orientation conditions 'left', 'straight' and 'right'. The body-head schemata indicate the head orientations. Data at the R peak (t_R) and at the T peak (t_T) (top and bottom respectively).

cardiac origin. The CFA is most prominent during the QRS complex and during the T wave. It changes rapidly during the QRS complex and more slowly during the T wave. At the R peak and at the T peak the potential patterns are distinctly asymmetrical with respect to the two hemispheres. At these two time points equipotential lines on the scalp are oriented diagonally from the left front to the right back of the head. The amplitudes of the CFA range from -10 to 10 μV.

All 9 subjects showed similar potential patterns. Features supporting the hypothesis of a mainly cardiac origin of the observed potential patterns are: (a) the asymmetry of the patterns and their synchronized rotation with the heart vector and (b) the existence of head turn effects in the form of rotation-like alterations of the potential patterns.

The CFA-free window during the post T interval allows the undisturbed study of heart cycle-related potentials. Interestingly, the attention-related effect described by Montoya et al. (1993) was found to be significant in a segment of the heart cycle that partially coincides with the CFA-free interval.

Moreover, a treatment of the CFA during the T wave is possible. The results indicate the existence of scalp regions that are strongly affected by the CFA and other regions in which the artifact appears to be rather small. A diagonally oriented region from a left frontal location (near T3, F7) to a right occipital location (near T4, T6) is hardly affected by the CFA. In contrast, the scalp regions over the frontal part of the right hemisphere and over the occipital part of the left hemisphere are strongly affected.

The shape and orientation of the CFA pattern can be altered experimentally by changing the spatial relations between the source of the artifact, the heart, and the location of measurement, the head. Head turns provide one method for altering the CFA while brain potentials remain unaltered.

The results of the head rotation experiment emphasize the geometrical complexity of the rules of propagation of the cardiac field through the body tissue towards the scalp (Hämäläinen et al., 1993). The observed rotation angles reached only about 45% of the magnitude of the angles by which the head was physically turned. Both assumptions

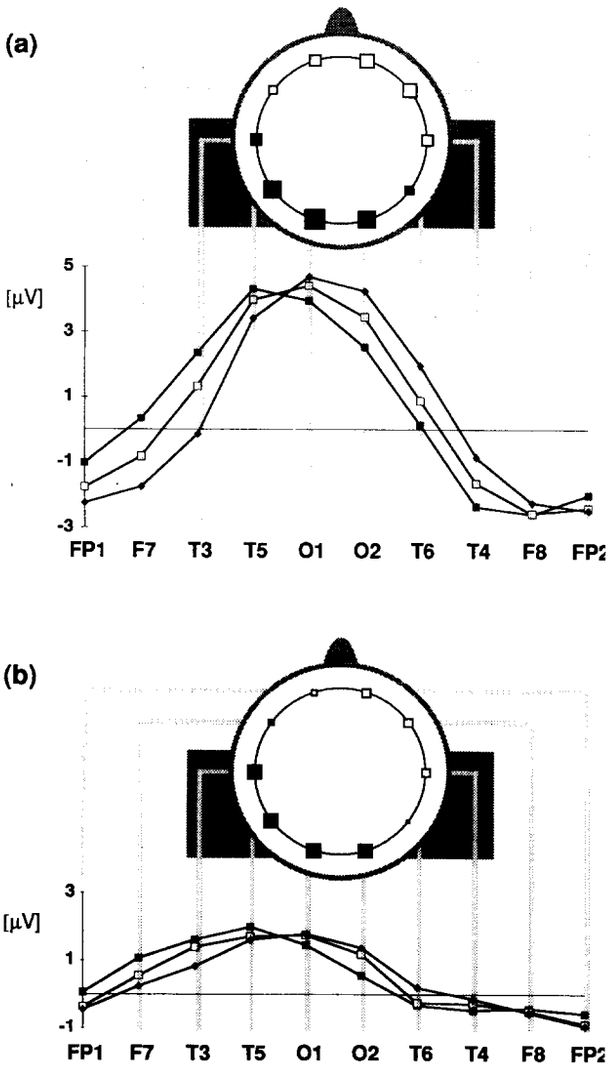

Fig. 6. Grand averages (n = 9) of potentials at the 10 electrode positions along the ring containing, in counterclockwise sequence, Fp1, F7, T3, T5, O1, O2, T6, T4, F8 and Fp2, observed in the three head orientation conditions. (a) At t_R: the head schema shows the group averaged potentials at the 10 positions along the ring in the 'straight' condition. These data correspond to the middle curve (open square) below. The curves for the 'left' (filled square), and 'right' (rhombus) head turn conditions are also shown. (b) At t_T: analogous to (a). However, t_T varies individually; the averaged data underlying this curve were measured at individually different latencies.

based on simple propagation models, namely a strictly body tissue-attached field propagation and a torso-related field propagation, are not in full accordance with this finding.

The amplitude of the CFA was found to increase markedly for electrode positions with shorter distances from the heart. In all subjects the maximal artifact amplitudes during the T wave were found at the positions Cb1 and Cb2 which are located at about 75% of the vertical distance between the heart and Cz. The reported results of regression analysis demonstrate that the CFA can be properly described only in a three-dimensional representation. Estimations of the CFA effects at different scalp locations from one-dimensional data are theoretically impossible. The very small signal-to-noise ratio for heart cycle-related brain potentials until after the complete decay of the T wave makes it practically impossible to use computational approaches to remove the CFA. Two major difficulties prohibit a practical solution of the forward problem of the CFA: the cardiac field cannot be measured in sufficient detail and the rules of propagation towards the scalp are still not known precisely enough.

Although the findings discussed here demonstrate the complexity of the CFA, they also suggest strategies for using cardiac cycle-related EEG averaging to study heart cycle-related brain potentials. Above all, non-computational methods can be used. Firstly, potentials in the refractory interval of the heart cycle are not confounded by the CFA. Yet, interindividual differences in the post-T wave interval must be taken into consideration. Secondly, low-artifact scalp regions exist where brain potentials can be assumed to be less confounded by the artifact. These regions can be altered by changing the spatial relations between the heart and the head, e.g. by head turns. However, the effects of head turns on the orientation of the low-artifact region were quantitatively not very prominent. They indicate an experimental uncoupling of the cardiac field artifact from brain potentials. Thirdly, comparisons of potentials obtained under identical conditions with regard to the cardiac field, i.e. above all under standardized heart-head spatial relations, are methodologically sound because the CFA can be eliminated by computing difference potentials. Although this paradigm also eliminates other identical potentials, e.g. brain potentials, it still allows a measurement of differential effects, c.f. attentional effects as described by Montoya et al. (1993).

In summary, the CFA must be regarded as an important factor that can mask heart cycle-related brain potentials if not properly treated. However, time windows exist during which the CFA is absent or negligibly small and paradigms can be used that combine data observed under different conditions so that differential effects on heart cycle-related brain potentials can be measured while CFA effects are cancelled out by interference. Cautiously applied, event-related EEG averaging can be an effective approach for assessing heart cycle-related information which can be utilized in the growing research activities on interoceptive processes in recent years (Reed et al., 1990; Jänig, 1995).

Acknowledgements

We thank Dr R. Haberl and Dr D. Kronski for advice on the cardiological aspects of the study and Dr J. Kamiya and Dr T. Pollmächer for valuable comments on the present paper.

References

Gratton, G., Coles, M.G.H. and Donchin, E. A new method for off-line removal of ocular artifact. Electroenceph. clin. Neurophysiol., 1983, 55: 468–484.

He, B. and Cohen, R.J. Body surface Laplacian ECG mapping [published erratum appears in IEEE Trans. Biomed. Eng., 1994, 41: 410]. IEEE Trans. Biomed. Eng., 1992, 39: 1179–1191.

Hämäläinen, M.S., Hari, R., Ilmoniemi, R.J., Knuutila, J.S. and Lounasmaa, O.V. Magnetencephalography – theory, instrumentation, and applications to noninvasive studies of the working human brain. Rev. Mod. Phys., 1993, 65: 537–571.

Heuser-Link, M., Dirlich, G., Berg, P., Vogl, L. and Scherg, M. Eyeblinks evoke potentials in the occipital brain region. Neurosci. Lett., 1992, 143: 31–34.

Jänig, W. Visceral afferent neurons: neuroanatomy and functions, organ regulations and sensations. In: D. Vaitl and R. Schandry (Eds.), From the Heart to the Brain: the Psychophysiology of Circulation–Brain Interaction. Peter Lang, Europäischer Verlag der Wissenschaften, Frankfurt am Main, 1995, pp. 5–34.

Jasper, H. Ten twenty electrode system of the international federation. Electroenceph. clin. Neurophysiol., 1958, 10: 371–375.

Jones, G.E., Leonberger, T.F., Rouse, C.H., Caldwell, J.A. and Jones, K.R. Preliminary data exploring the presence of an evoked potential associated with cardiac visceral activity [abstract]. Psychophysiology, 1986, 23: 445.

Jones, G.E., Rouse, C.H. and Jones, K.R. The presence of visceral evoked potentials elicited by cutaneous palpation of heartbeats in high and low awareness subjects [abstract]. Psychophysiology, 1988, 25: 459.

Lorange, M. and Guirajani, R.M. A computer heart model incorporating anisotropic propagation. I. Model construction and simulation of normal activation. J. Electrocardiol., 1993, 26: 245–261.

Medvegy, M., Antaloczy, Z. and Cserjes, Z. A new possibility in the study of heart activation: the nondipolar body surface map. Can. J. Cardiol., 1993, 9: 215–218.

Montoya, P., Schandry, R. and Mueller, A. Heartbeat evoked potentials (HEP): topography and influence of cardiac awareness and focus of attention. Electroenceph. clin. Neurophysiol., 1993, 88: 163–172.

Reed, S.D., Harver, A. and Katkin, E.S. Interoception. In: J.T. Cacioppo and L.G. Tassinary (Eds.), Principles of Psychophysiology. Physical, Social, and Inferential Elements. Cambridge University Press, Cambridge, 1990.

Riordan, H., Squires, N.K. and Brener, J. Cardio-cortical potentials: electrophysiological evidence for visceral perception [abstract]. Psychophysiology, 1990, 27: S59.

Sandman, C.A., Vigor-Zierk, C.S., Isenhart, R., Wu, J. and Zetin, M. Cardiovascular phase relationships to the cortical event-related potential of schizophrenic, depressed, and normal subjects. Biol. Psychiatry, 1992, 32: 778–789.

Schandry, R., Sparrer, B. and Weitkunat, R. From the heart to the brain: a study of heartbeat contingent scalp potentials. Int. J. Neurosci., 1986, 30: 261–275.

Schandry, R. and Weitkunat, R. Enhancement of heartbeat-related brain potentials through cardiac awareness training. Int. J. Neurosci., 1990, 53: 243–253.

Scherg, M. Fundamentals of dipole source analysis. In: F. Grandori, M. Hoke and G.L. Romani (Eds.), Auditory Evoked Magnetic Fields and Electric Potentials, Advances in Audiology, Vol. 6. Karger, Basel, 1990.

Slant, R.C. and Alexander, R.W. (Eds.). Hurst's the Heart: Arteries and Veins, 8th edn. McGraw Hill, New York, 1994.

Turzova, M., Tysler, M. and Kneppo, P. A model study of the sensitivity of body surface potential distribution to variations of electrode placement. J. Electrocardiol., 1994, 27: 255–262.

Walker, B.B. and Sandman, C.A. Visual evoked potentials change as heart rate and carotid pressure change. Psychophysiology, 1982, 19: 520–527.